Hard X-Ray Nanofocusing with Refractive X-Ray Optics: Full Beam Characterization by Ptychographic Imaging

Christian G. Schroer[a], Florian-Emanuel Brack[a], Roman Brendler[a], Susanne Hönig[a], Robert Hoppe[a], Jens Patommel[a], Stephan Ritter[a], Maria Scholz[a], Andreas Schropp[a], Frank Seiboth[a], Daniel Nilsson[b], Jussi Rahomäki[b], Fredrik Uhlén[b], Ulrich Vogt[b], Juliane Reinhardt[c], Gerald Falkenberg[c]

[a]Institute of Structural Physics, Technische Universität Dresden, D-01062 Dresden, Germany;
[b]Department of Applied Physics, KTH/Royal Institute of Technology, SE-10691 Stockholm, Sweden;
[c]Photon Science, DESY, Notkestr. 85, D-22607 Hamburg, Germany

ABSTRACT

Hard x-ray scanning microscopy relies on small and intensive nanobeams. Refractive x-ray lenses are well suited to generate hard x-ray beams with lateral dimensions of 100 nm and below. The diffraction limited beam size of refractive x-ray lenses mainly depends on the focal length and the attenuation inside the lens material. The numerical aperture of refractive lenses scales with the inverse square root of the focal length until it reaches the critical angle of total reflection. We have used nanofocusing refractive x-ray lenses made of silicon to focus hard x-rays at 8 and 20 keV to (sub-)100 nm dimensions. Using ptychographic scanning coherent diffraction imaging we have characterized these nanobeams with high accuracy and sensitivity, measuring the full complex wave field in the focus. This gives access to the full caustic and aberrations of the x-ray optics.

Keywords: hard x-ray nanobeam, nanofocusing refractive x-ray lenses, ptychography, beam characterization

1. INTRODUCTION

X-ray scanning microscopy is a growing field with applications in many fields of science, such as physics, chemistry, biomedicine, materials-, earth- and environmental science, and nanotechnology. The main advantage of x-ray microscopy over other microscopy techniques is the large penetration depth of x rays in matter. This allows one to probe the interior of a specimen without destructive sample preparation and to image objects inside of special sample environments, such as chemical reactors, microfluidic or pressure cells. For example, catalytic reactions can be followed under operating conditions.[1]

In x-ray scanning microscopy the sample is scanned through a laterally confined x-ray beam. At each position of the scan, x-ray analytical techniques, such as x-ray fluorescence analysis, x-ray absorption spectroscopy, or x-ray diffraction, can be applied locally to the sample. This allows one to map, for example, the element distribution, the chemical state of an element of interest, or the local atomic structure, respectively. By combining these scanning techniques with tomography local information from inside the specimen can be obtained.[2–7]

Scanning microscopy requires a small and intensive x-ray beam that is generated by focusing the x-ray source onto the sample using an x-ray focusing optic. X-ray scanning microscopy greatly benefits from the high brilliance of modern synchrotron radiation sources. Over the last two decades, significant progress has been made in the field of x-ray optics, pushing the diffraction limit of diffractive,[8–13] reflective,[14,15] and refractive x-ray optics well below the 100 nm level.[16,17]

As the x-ray beams become ever smaller, their characterization becomes more and more challenging. In recent years, ptychography has revolutionized the characterization of x-ray optics.[18–20] For optics characterization, a test object is typically scanned through the nanobeam in two lateral dimensions, recording at each scanning

Further author information: (Send correspondence to Christian G. Schroer)
Christian G. Schroer: E-mail: schroer@xray-lens.de, Telephone: +49 (351) 463 37589

Advances in X-Ray/EUV Optics and Components VIII, edited by Ali Khounsary, Shunji Goto, Christian Morawe, Proc. of SPIE Vol. 8848, 884807 · © 2013 SPIE
CCC code: 0277-786X/13/$18 · doi: 10.1117/12.2024127

Downloaded From: http://proceedings.spiedigitallibrary.org/ on 10/07/2013 Terms of Use: http://spiedl.org/terms

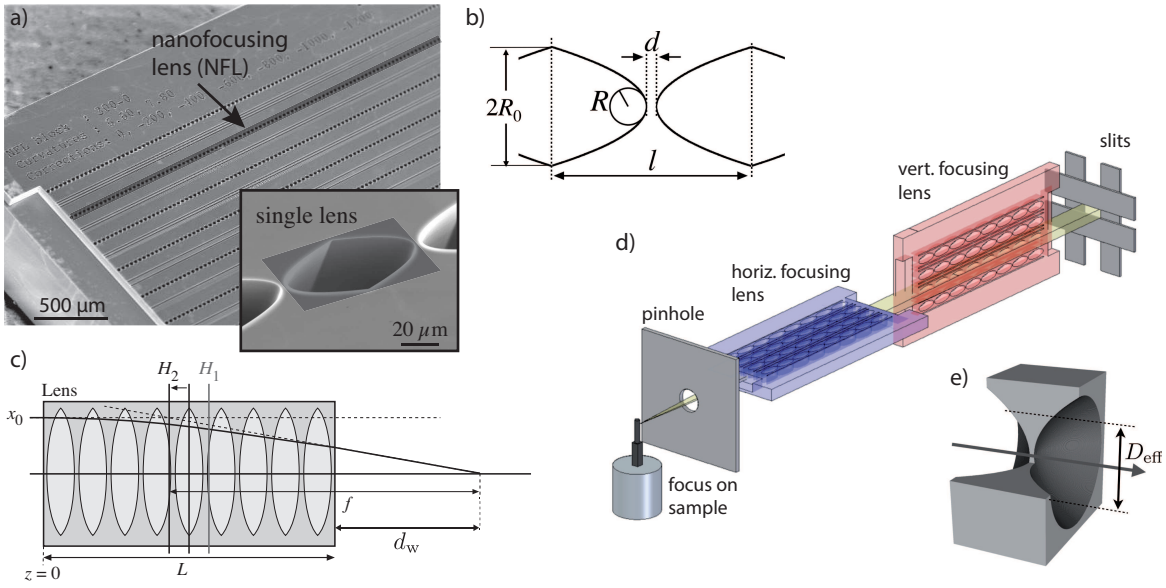

Figure 1. a) Nano focusing refractive x-ray lenses (NFLs) made of silicon. Several NFLs with different parameters are placed side by side on the same wafer. The inset shows a detail of a nano focusing lens, highlighting one single lens. b) geometric parameters of a single refractive lens, c) focusing by an optically thick nanofocusing refractive lens. Each ray follows approximately a short segment of a sinusoidal path inside the lens. d) Schematic setup of a nano probe based on NFLs: two NFLs are aligned behind each other in crossed geometry. The incident beam is restricted to the aperture of the NFLs by a pair of slits. Behind the NFLs, the focused beam is singled out by a pinhole, removing scattered radiation. The two lenses are aligned such as to generate a point focus at the sample position. e) Rotationally parabolic refractive lens with the effective aperture D_{eff} that is reduced compared to the geometric aperture due to increased attenuation of peripheral rays.

position a far-field diffraction pattern of the illuminated area of the object. From these data, both the object's complex transmission function and the complex wave field of the nanobeam at the position of the object can be reconstructed. By numerically propagating the complex wave field along the optical axis, the full beam caustic can be reconstructed. In this way, the full spatial wave function of the x rays (solution to the Helmholtz equation) can be obtained, also giving access to the exit wave field behind the optic and thus its aberrations. Ptychography is very sensitive and can measure the intensity distribution with a dynamic range of at least four orders of magnitude.[20]

The technique has been applied to various x-ray optics[11,20–23] and is by now routinely applied for aligning and characterizing hard x-ray nanobeams at the Hard X-ray Micro/Nano-Probe Beamline P06[24] at the synchrotron radiation source PETRA III at DESY in Hamburg, Germany. The reliability of this approach has been verified by S. Hönig, et al..[25]

In this article, we review the optical properties and physical limitations of nanofocusing refractive x-ray lenses (NFLs).[16,26] We characterize nanobeams generated by NFLs made of silicon at 8 keV and 20 keV using ptychographic imaging. At 8 keV the optic's aperture is limited by attenuation inside the lens material. This limits the size of the aperture and thus the size of the Airy disc (beam size: 175 nm). At the same time the optic has a nearly ideal Gaussian aperture function, leading to an almost ideal Gaussian diffraction limited beam. At 20 keV the attenuation inside the lens is smaller, leading to a diffraction limited beam of 55 nm in size.

2. NANOFOCUSING REFRACTIVE X-RAY OPTICS

Refractive lenses for hard x-rays typically consist of a series of optically thin individual lenses stacked behind each other to form a compound lens.[27] Fig. 1a) shows several nanofocusing lenses (NFLs) made of silicon next to each other on a silicon wafer.[16,26] The inset shows a single lens. For thin optics in paraxial approximation, the

Downloaded From: http://proceedings.spiedigitallibrary.org/ on 10/07/2013 Terms of Use: http://spiedl.org/terms

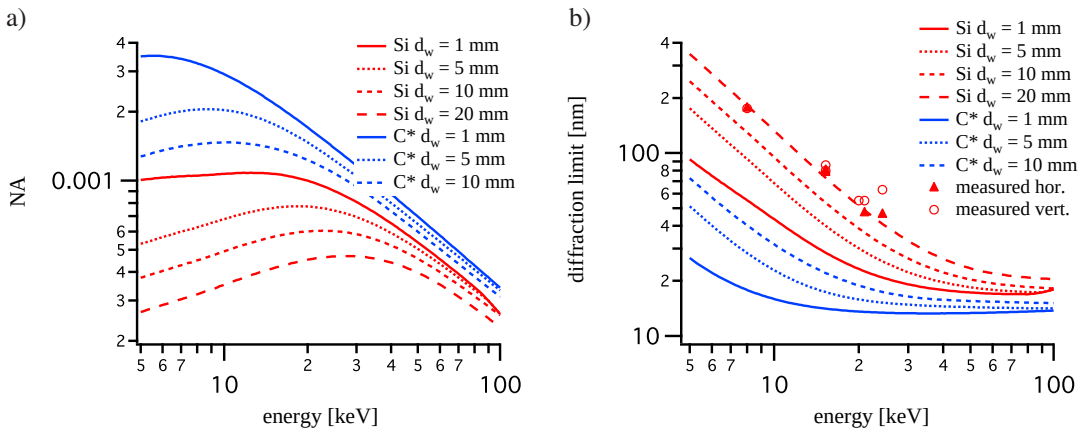

Figure 2. a) Numerical aperture and b) corresponding diffraction limit of nanofocusing refractive lenses made of silicon and diamond optimized for different working distances. In current x-ray microscopes, a practical working distance is approximately 10 mm and above. Some measured diffraction limited focal spot sizes are shown in b).[16,17,20,30]

ideal shape of the lens surfaces is a parabola. As the paraxial and thin lens approximations are both excessively well fulfilled for each single refractive lens in the hard x-ray range, the parabolic shape is optimal for these lenses. The spherical approximation, however, does not hold for these strongly curved lenses* and the parabolic shape is crucial to avoid spherical aberrations and to achieve diffraction limited focusing.[28]

The aperture function of a refractive x-ray lens is typically a truncated Gaussian, i. e., inside the lens aperture up to the geometric aperture radius R_0, the wave field is attenuated according to a Gaussian transmission function, while it is zero outside the geometric aperture. To make the aperture as large as possible, the geometric aperture should cut as little of the amplitude as possible. In this case, the attenuation dominates the transmission through the optic, and the effective aperture is

$$D_{\text{eff}} = 4 \cdot \sqrt{f \cdot \frac{\delta}{\mu}} \propto \sqrt{f \cdot E}, \tag{1}$$

where f is the focal length, δ is the index of refraction decrement (index of refraction: $n = 1 - \delta + i\beta$), and $\mu = 4\pi\beta/\lambda$ is the attenuation coefficient of the material. At fixed focal length f, D_{eff} scales approximately proportional to $\sqrt{E}$. For a strongly focusing geometry, i. e., the object distance L_1 is much larger than the focal length f, the numerical aperture is

$$NA = \frac{D_{\text{eff}}}{2 \cdot f} \propto \sqrt{\frac{E}{f}}, \tag{2}$$

and the full-width-at-half-maximum (FWHM) diffraction limited beam size d_t is determined by Abbe's formula for a Gaussian Airy disc:

$$d_t = \alpha \cdot \frac{\lambda}{2NA} \propto \sqrt{\frac{f}{E^3}}. \tag{3}$$

Here, λ is the wavelength of the x rays and $\alpha \approx 0.75$.[29] In order to minimize the diffraction limit, it is thus advantageous to reduce the focal length as much as possible for a given energy. This argument led to the development of refractive lenses with short focal length, i. e., nanofocusing lenses (NFLs).[16,26]

For smaller and smaller focal length, the compound lens becomes increasingly optically thick.† Its overall

*In spherical approximation, the radius R has to be much larger than the aperture radius R_0.

†The individual lenses in the compound lens are optically thin, and the parabolic shape for individual lens surfaces remains optimal.

Downloaded From: http://proceedings.spiedigitallibrary.org/ on 10/07/2013 Terms of Use: http://spiedl.org/terms

length L eventually limits the focal length that is given by

$$f = \frac{1}{\omega \sin(\omega L)}, \quad \omega^2 = \frac{2\delta}{lR} \approx \frac{2\delta}{R_0^2},$$

where ω^2 is the refractive power per unit length given by the parameters defined in Fig. 1b). The working distance is [cf. Fig. 1c)]

$$d_{\mathrm{w}} = \frac{R_0 \cdot \cos(\omega L)}{R_0 \cdot \omega \cdot \sin(\omega L)} = \frac{1}{\omega} \cot(\omega L).$$

Decreasing the focal length eventually requires a reduction of the length L of the compound lens that is accompanied by a reduction of the geometric aperture radius R_0. For sufficiently small f, the geometric aperture radius R_0 cuts into the Gaussian aperture, eventually becoming the limiting parameter for the numerical aperture. In this regime, the aperture is no longer determined by the attenuation inside the lens material, and the numerical aperture and the diffraction limit approach

$$NA = \frac{\sqrt{2\delta}}{\sin(\omega L)} \propto \frac{1}{E}, \quad \Rightarrow \quad d_t = \alpha \cdot \frac{\lambda}{2\sqrt{2\delta}} \cdot \sin(\omega L) \propto \mathrm{const.} \tag{4}$$

for a fixed imaging geometry. Highest numerical apertures are reached, when $\sin(\omega L) \to 1$, i. e., the focus lies directly at the exit of the lens and the working distance $d_{\mathrm{w}} = 0$. In that case, the numerical aperture approaches the critical angle of total reflection [cf. eq. (4)].[26]

Fig. 2 shows the numerical aperture NA and the diffraction limit d_t for nanofocusing lenses made of silicon and diamond for different working distances. The shortest focal lengths and thus shortest working distances yield largest numerical apertures and smallest diffraction limits. Practical considerations typically limit the working distance in an x-ray scanning microscope to 10 mm and above. In particular, the vertically focusing lens [cf. Fig. 1c)] has a larger working distance. At lower energies, attenuation effects inside the NFLs limit the numerical aperture and spatial resolution (cf. Fig. 2). At higher energies, i. e., above 10 to 20 keV for diamond and above 30 to 40 keV for silicon, the NFLs are in the non-absorptive limit.

Ultimately, in the low-attenuation limit, nanofocusing lenses are limited in numerical aperture by the critical angle of total reflection $\sqrt{2\delta}$,[26,31] where the refractive index decrement is

$$\delta = \frac{N_{\mathrm{A}}}{2\pi} \cdot r_0 \cdot \rho \cdot \lambda^2 \cdot \frac{f(0)}{A}. \tag{5}$$

Here, N_{A} is Avogradro's constant, r_0 is the classical electron radius, ρ is the density, $f(q=0) \approx Z$ the atomic form factor in forward direction (Z: atomic number), and A the atomic mass of the lens material. According to eq. (4), the diffraction limit is thus bounded by

$$d_t = \alpha \cdot \frac{1}{2\sqrt{\frac{N_{\mathrm{A}}}{\pi} \cdot r_0 \cdot \frac{Z}{A}}} \cdot \frac{1}{\sqrt{\rho}} \approx \mathrm{const.} \cdot \frac{1}{\sqrt{\rho}}$$

that is nearly independent of the lens material. The optimal diffraction limit only depends on the density of the material.

3. PTYCHOGRAPHIC IMAGING WITH THE HARD X-RAY SCANNING MICROSCOPE AT BEAMLINE P06 AT PETRA III

The hard x-ray scanning microscope[24] of beamline P06 at PETRA III at DESY is in user operation since the beginning of 2012. It is based on nanofocusing refractive x-ray lenses and provides x-ray fluorescence, x-ray absorption, and (coherent) x-ray diffraction contrast.[30,32] Ptychography is one of the standard techniques available at this instrument and is routinely used to align the optics and characterize the nanobeam for all experiments.

Downloaded From: http://proceedings.spiedigitallibrary.org/ on 10/07/2013 Terms of Use: http://spiedl.org/terms

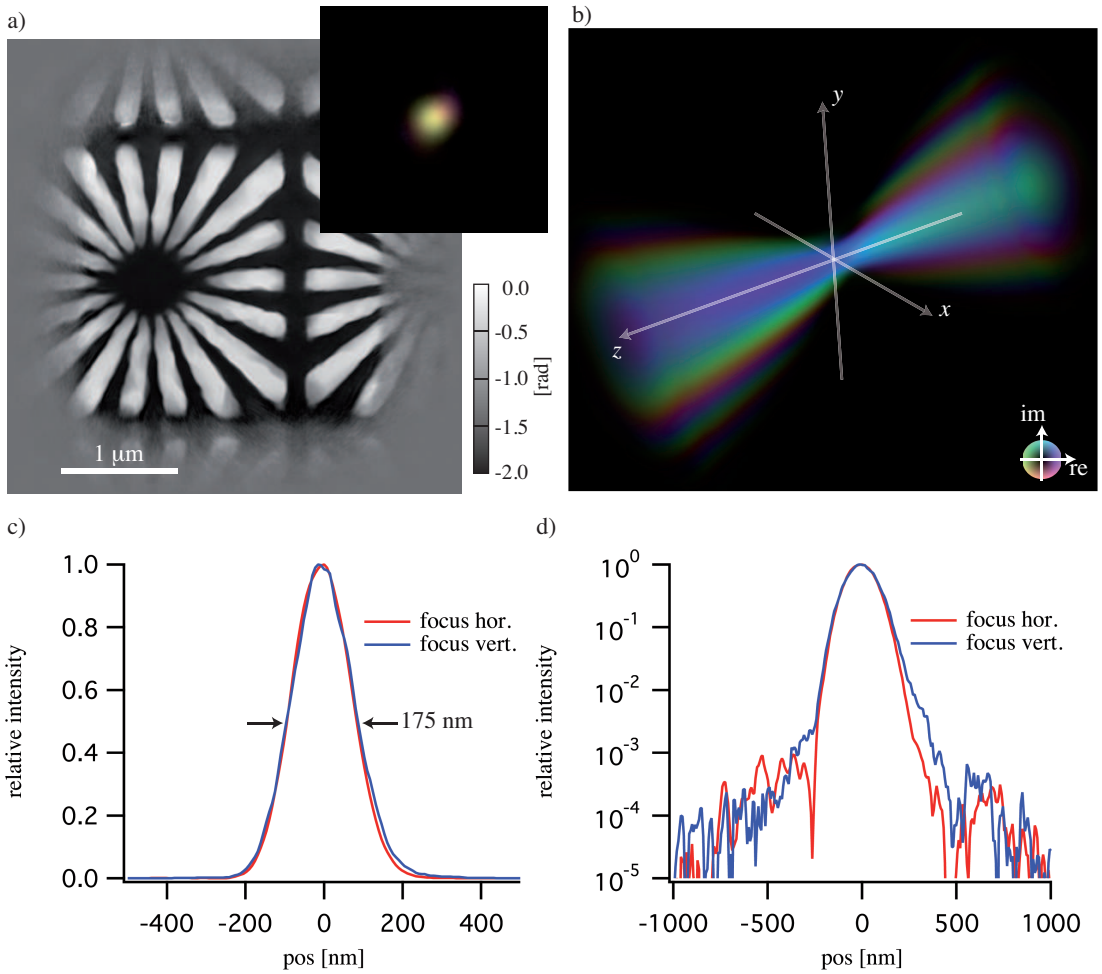

Figure 3. a) Ptychographic reconstruction of test object and illumination for a nanobeam made with NFLs at $E = 8$ keV. b) The reconstructed complex illumination function propagated along the optical axis (range −4 mm to 4 mm) using the Fresnel-Kirchhoff integral. The lateral intensity distribution in the focus shown in c) and d) is nearly Gaussian with a full-width-half-maximum width of 175 nm, both horizontally and vertically. The logarithmic representation in d) shows the absence of side maxima down to a relative intensity of 10^{-3}.

The x-ray scanning microscope is located at about 98 m from the undulator source. A Si (111) double-crystal monochromator is used to monochromatize the beam. Higher undulator harmonics are rejected using a pair of total reflection mirrors with different coatings (Si, Cr, Pt). The x rays are focused by a set of crossed nanofocusing refractive x-ray lenses [cf. Fig. 1d)]. The flux and the degree of coherence is adjusted by prefocusing lenses located at about 43.3 m behind the undulator. For high-coherence applications, such as ptychography, the beam is usually not prefocused.

The nanobeam is characterized by ptychography using a strongly scattering test object as a sample. The sample is scanned through the beam in horizontal and vertical translation perpendicular to the beam, recording at each position of the scan a far-field diffraction pattern with a Pilatus 300k pixel detector by Dectris, Baden, Switzerland. The data are then reconstructed by a ptychographic reconstruction engine based on the algorithm described by A. Maiden and J. Rodenburg.[33] With a GPU version of this software available at the beamline, the reconstruction is fast enough to use the method for the alignment of the optics and the sample.

Downloaded From: http://proceedings.spiedigitallibrary.org/ on 10/07/2013 Terms of Use: http://spiedl.org/terms

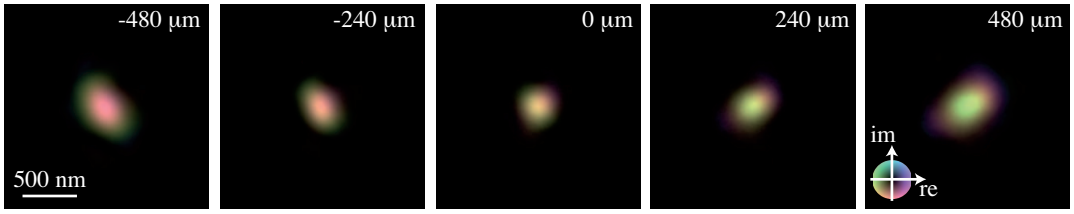

Figure 4. Defocus series reconstructed for the nanobeam at 8 keV, showing a slight astigmatism with principal axes diagonal to the pair of nanofocusing lenses. This type of astigmatism is typical for a slight misalignment of the nanofocusing lenses with respect to each other: the cylindrical lenses are not perfectly perpendicular to each other.

4. GAUSSIAN NANOBEAM AT 8 KEV

We have characterized the beam obtained by focusing 8 keV x rays with nanofocusing lenses made of silicon. Two NFLs with $N = 35$ individual lenses and a radius of curvature at the apex of $R = 8$ μm and $R = 10$ μm were used to focus the x rays in horizontal and vertical direction, respectively [cf. Fig. 1d)]. The design thickness of individual lenses at their apex is $d = 1.5$ μm. At this energy, the aperture of these optics is dominated by the attenuation inside the silicon, leading to an effective aperture of $D_{\mathrm{eff}} = 11.3$ μm and 12.6 μm, respectively. For comparison, the geometric apertures of these two optics are $2R_0 = 30.2$ μm and 35.7 μm, respectively. At the geometric aperture, the intensity is reduced by a factor $6 \cdot 10^{-7}$ compared to the intensity on the optical axis. Thus the aperture is nearly perfectly Gaussian. The working distance of the two optics is 14.5 mm and 18.25 mm, respectively, and the expected diffraction limited focus size is 156×174 nm^2 (H×V, FWHM).

With this beam a ptychogram was recorded, scanning a periodic test pattern with star-like motif over a range of 2×2 μm^2 in 25×25 steps of 80×80 nm^2. The test pattern is made of tungsten (thickness ≈ 1 μm) on a diamond substrate (thickness 100 μm). The far-field diffraction patterns were recorded by a Pilatus 300k pixel detector (pixel size: 172 μm) that was located at a distance of 2080 mm behind the object (exposure time: 1 s).

Fig. 3a) shows the reconstructed phase of the test pattern (pixel size: 7.32 nm) together with the complex wave field of the illuminating beam (inset). The wave field can be propagated along the optical axis using the Fresnel-Kirchhoff integral. The resulting three-dimensional complex wave field is shown in Fig. 3b) in a range of -4 to 4 mm around the focus. From these data, the beam profile in the focus can be extracted [Fig. 3c),d)], having a FWHM beam width of 175×175 nm^2. The profile is Gaussian over about three orders of magnitude in intensity as shown in Fig. 3d). Horizontally, there is a slight discrepancy between the expected optimal (156 nm) and the measured focus (175 nm). This can be explained by a slight misalignment of the lenses with respect to each other that introduces a slight astigmatism shown in Fig. 4. Over 80% of the radiation lies within a radius of 100 nm, 95% within a radius of 150 nm. There are no side maxima visible in the reconstruction.

5. NANOBEAM AT 20 KEV

Fig. 2 shows that the focusing properties of nanofocusing lenses made of silicon are dominated by attenuation inside the lens' aperture below 30 keV. This effect is particularly pronounced below 10 keV, where the transmission and numerical aperture are significantly reduced compared to the optimum. Therefore, nanofocusing lenses made of silicon are seldom operated below 10 keV as in the example shown in the previous section. Here, we show an example of a nanobeam at $E = 20$ keV. At this energy, the attenuation inside the lens aperture is already quite reduced and the numerical aperture is close to its optimum [cf. Fig. 2a)].

We recorded a ptychogram of the nanobeam generated by a silicon nanofocusing lens with $N = 300$ single lenses with a radius of curvature of $R = 12.6$ μm crossed with an adiabatically focusing lens.[34] At $E = 20$ keV the lens has a focal length of $f = 19$ mm and thus a working distance $d_{\mathrm{w}} = 14.3$ mm. A Siemens-star test pattern made of tantalum (NTT-AT, Japan) was scanned through the nanobeam over a field of view of 2×2 μm^2 in 100×100 steps of 20×20 nm^2. At each position of the scan a far-field diffraction pattern was recorded with the Pilatus 300K pixel detector located at a distance of 2222 mm behind the sample.

Fig. 5a) shows the projected intensity along the horizontal direction in the range of -0.5 to 0.5 mm. The beam is nearly Gaussian with a FWHM width of 55 nm [cf. Fig. 5b)]. The effective aperture $D_{\mathrm{eff}} = 19.6$ μm is

Downloaded From: http://proceedings.spiedigitallibrary.org/ on 10/07/2013 Terms of Use: http://spiedl.org/terms

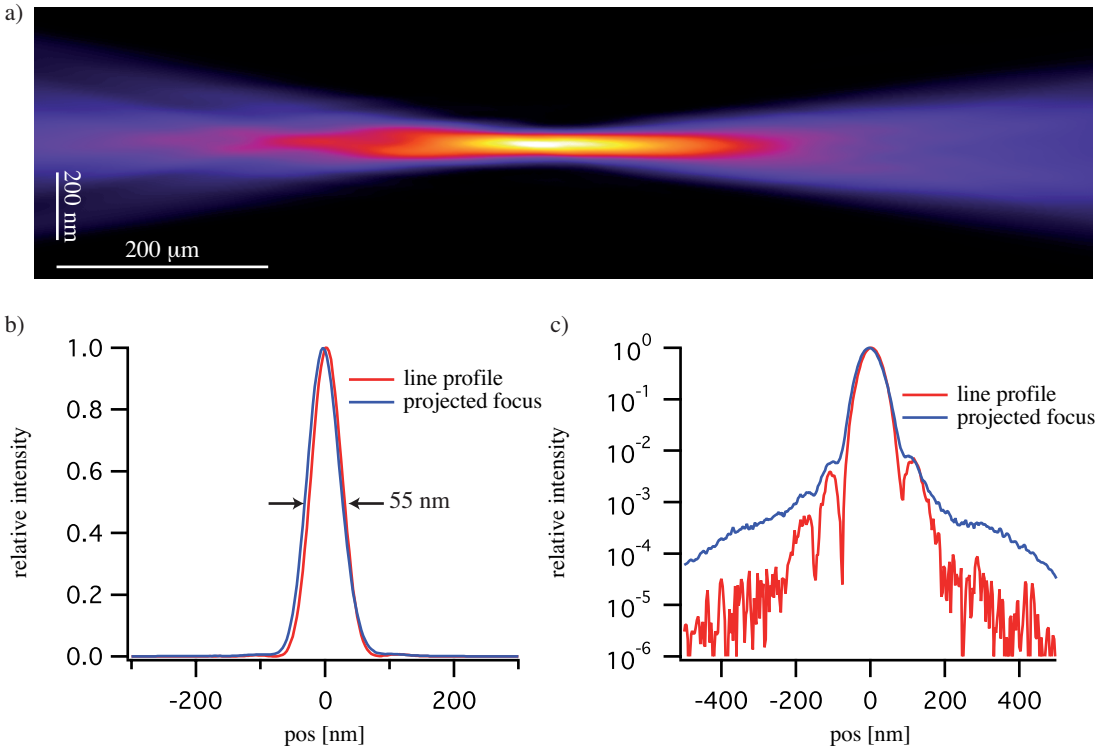

Figure 5. a) Reconstructed caustic (vertical beam profile) of a nanobeam generated at $E = 20$ keV by a nanofocusing lens. It is made of $N = 300$ single lenses with a radius of curvature of $R = 12.6$ μm. With a focal length of $f = 19$ mm, the focus is formed 14.3 mm behind the optic. Line profile and the focus projected along the horizontal axis on linear a) and logarithmic scale b). The focus is nearly Gaussian and its full-width-half-maximum beam size is 55 nm. Outside of the focus, the relative intensity drops quickly to the noise level of the measurement of about 10^{-5}. 94% of the radiation lie within an interval of 100 nm around the focus, 66% of the radiation lie within 50 nm.

about half the size of the geometric aperture $2R_0 = 38$ μm, and the aperture function is nearly Gaussian. The truncation of the Gaussian at the geometric aperture is nearly negligible, as the intensity at the periphery of the lens is reduced by $2.6 \cdot 10^{-4}$ relative to that of the central beam. Nevertheless, side maxima are visible in the intensity on a logarithmic scale [Fig. 5c)].

6. CONCLUSION AND OUTLOOK

Due to their "soft" aperture, nanofocusing refractive x-ray lenses can generate nearly Gaussian diffraction limited nanobeams in the hard x-ray range. They are used in hard x-ray scanning microscopes at PETRA III in Hamburg and at the European Synchrotron Radiation Facility (ESRF) in Grenoble, France. Their numerical aperture and thus the achievable diffraction limit improves with decreasing focal length, eventually being limited by the critical angle of total reflection that depends mainly on the density of the lens material. A prerequisite to high numerical aperture is a small attenuation in the lens material. This implies the use of lens materials with low atomic number Z. Diamond is the ideal material, as it combines low Z with relatively high density. For technological reasons, nanofocusing lenses made of silicon show the best experimental performance, today.

Diffraction limited focusing implies a high degree of coherence in the focus.[35] Therefore, coherent x-ray diffraction imaging techniques work well with these beams, and ptychography is ideally suited for high-resolution

Downloaded From: http://proceedings.spiedigitallibrary.org/ on 10/07/2013 Terms of Use: http://spiedl.org/terms

imaging and to characterize the beam. Indeed, ptychography has revolutionized the characterization of diffraction limited hard x-ray nanobeams in several ways: being able to reconstruct the full complex wave field gives access to the full caustic of the beam and yields easy-to-interpret three-dimensional beam profiles as opposed to one-dimensional projections given for example by knife-edge techniques. In addition, the method can be easily scaled to ever smaller beams and the ptychographic measurement can be made at a distance from the point of interest along the optical axis. In this way, the beam can be characterized even at positions along the optical axis that are not directly accessible, such as the exit aperture of a wave guide.

ACKNOWLEDGMENTS

The authors thank D. Samberg for his excellent technical support. Beamtime at PETRA III was granted within the user programme. This work is supported by the German Ministry of Education and Research (BMBF) under grant number 05K10OD1, by VH-VI-403 of the Impuls- und Vernetzungsfonds (IVF) of the Helmholtz Association of German Research Centres, the Swedish Research Council, and the Göran Gustafsson Foundation. The GPU implementation of the numerical algorithms is being developed within the NVIDIA CUDA Center of Excellence at Technische Universität Dresden.

REFERENCES

1. J.-D. Grunwaldt and C. G. Schroer, "Hard and soft x-ray microscopy and tomography in catalysis: Bridging the different time and length scales," *Chem. Soc. Rev.* **39**, p. 4741, 2010.
2. A. S. Simionovici, M. Chukalina, C. Schroer, M. Drakopoulos, A. Snigirev, I. Snigireva, B. Lengeler, K. Janssens, and F. Adams, "High-resolution x-ray fluorescence microtomography of homogeneous samples," *IEEE Trans. Nucl. Sci.* **47**(6), pp. 2736–2740, 2000.
3. C. G. Schroer, "Reconstructing x-ray fluorescence microtomograms," *Appl. Phys. Lett.* **79**(12), pp. 1912–1914, 2001.
4. C. G. Schroer, M. Kuhlmann, T. F. Günzler, B. Lengeler, M. Richwin, B. Griesebock, D. Lützenkirchen-Hecht, R. Frahm, E. Ziegler, A. Mashayekhi, D. Haeffner, J.-D. Grunwaldt, and A. Baiker, "Mapping the chemical states of an element inside a sample using tomographic x-ray absorption spectroscopy," *Appl. Phys. Lett.* **82**(19), pp. 3360–3362, 2003.
5. C. G. Schroer, M. Kuhlmann, S. V. Roth, R. Gehrke, N. Stribeck, A. Almendarez-Camarillo, and B. Lengeler, "Mapping the local nanostructure inside a specimen by tomographic small angle x-ray scattering," *Appl. Phys. Lett.* **88**(16), p. 164102, 2006.
6. P. Bleuet, E. Welcomme, E. Dooryhée, J. Susini, J.-L. Hodeau, and P. Walter, "Probing the structure of heterogeneous diluted materials by diffraction tomography," *Nature Materials* **7**(6), pp. 468–472, 2008.
7. M. Kuhlmann, J. M. Feldkamp, J. Patommel, S. V. Roth, A. Timmann, R. Gehrke, P. Müller-Buschbaum, and C. G. Schroer, "Grazing incidence small-angle x-ray scattering microtomography on a self-ordered dried drop of nanoparticles," *Langmuir Lett.* **25**(13), pp. 7241–7243, 2009.
8. Y. S. Chu, J. M. Yi, F. De Carlo, Q. Shen, W.-K. Lee, H. J. Wu, C. L. Wang, J. Y. Wang, C. J. Liu, C. H. Wang, S. R. Wu, C. C. Chien, Y. Hwu, A. Tkachuk, W. Yun, M. Feser, K. S. Liang, C. S. Yang, J. H. Je, and G. Margaritondo, "Hard-x-ray microscopy with Fresnel zone plates reaches 40 nm Rayleigh resolution," *Appl. Phys. Lett.* **92**, p. 103119, Jan 2008.
9. H. C. Kang, H. Yan, R. P. Winarski, M. V. Holt, J. Maser, C. Liu, R. Conley, S. Vogt, A. T. Macrander, and G. B. Stephenson, "Focusing of hard x-rays to 16 nanometers with a multilayer laue lens," *Appl. Phys. Lett.* **92**, p. 221114, Jan 2008.
10. H. Mimura, S. Handa, T. Kimura, H. Yumoto, D. Yamakawa, H. Yokoyama, S. Matsuyama, K. Inagaki, K. Yamamura, Y. Sano, K. Tamasaku, Y. Nishino, M. Yabashi, T. Ishikawa, and K. Yamauchi, "Breaking the 10 nm barrier in hard-X-ray focusing," *Nature Physics* **6**, pp. 122–125, 2010.
11. J. Vila-Comamala, A. Diaz, M. Guizar-Sicairos, A. Mantion, C. M. Kewish, A. Menzel, O. Bunk, and C. David, "Characterization of high-resolution diffractive x-ray optics by ptychographic coherent diffractive imaging," *Opt. Express* **19**(22), pp. 21333–21344, 2011.

Downloaded From: http://proceedings.spiedigitallibrary.org/ on 10/07/2013 Terms of Use: http://spiedl.org/terms

12. H. Mimura, T. Kimura, H. Yumoto, H. Yokoyama, H. Nakamori, S. Matsuyama, K. Tamasaku, Y. Nishino, M. Yabashi, and T. Ishikawa, "One-dimensional sub-10-nm hard X-ray focusing using laterally graded multilayer mirror," *Nucl. Instrum. Methods A* **635**, pp. S16–S18, 2011.
13. H. Yan, V. Rose, D. Shu, E. Lima, H. C. Kang, R. Conley, C. Liu, N. Jahedi, A. T. Macrander, G. B. Stephenson, M. Holt, Y. S. Chu, M. Lu, and J. Maser, "Two dimensional hard x-ray nanofocusing with crossed multilayer laue lenses," *Opt. Express* **19**(16), pp. 15069–15076, 2011.
14. A. Jarre, C. Fuhse, C. Ollinger, J. Seeger, R. Tucoulou, and T. Salditt, "Two-dimensional hard x-ray beam compression by combined focusing and waveguide optics," *Phys. Rev. Lett.* **94**, p. 074801, 2005.
15. H. Mimura, H. Yumoto, S. Matsuyama, Y. Sano, K. Yamamura, Y. Mori, M. Yabashi, Y. Nishino, K. Tamasaku, T. Ishikawa, and K. Yamauchi, "Efficient focusing of hard x rays to 25 nm by a total reflection mirror," *Appl. Phys. Lett.* **90**(5), p. 051903, 2007.
16. C. G. Schroer, O. Kurapova, J. Patommel, P. Boye, J. Feldkamp, B. Lengeler, M. Burghammer, C. Riekel, L. Vincze, A. van der Hart, and M. Küchler, "Hard x-ray nanoprobe based on refractive x-ray lenses," *Appl. Phys. Lett.* **87**(12), p. 124103, 2005.
17. C. G. Schroer, A. Schropp, P. Boye, R. Hoppe, J. Patommel, S. Hönig, D. Samberg, S. Stephan, S. Schöder, M. Burghammer, G. Wellenreuther, and G. Falkenberg, "Hard x-ray scanning microscopy with coherent diffraction contrast," in *The 10th International Conference on X-Ray Microscopy*, I. McNulty, C. Eyberger, and B. Lai, eds., *AIP Conference Proceedings* **1365**, pp. 227–230, AIP, (Melville, New York), 2011.
18. J. M. Rodenburg and H. M. L. Faulkner, "A phase retrieval algorithm for shifting illumination," *Appl. Phys. Lett.* **85**(20), pp. 4795–4797, 2004.
19. P. Thibault, M. Dierolf, A. Menzel, O. Bunk, C. David, and F. Pfeiffer, "High-resolution scanning x-ray diffraction microscopy," *Science* **321**(5887), pp. 379–382, 2008.
20. A. Schropp, P. Boye, J. M. Feldkamp, R. Hoppe, J. Patommel, D. Samberg, S. Stephan, K. Giewekemeyer, R. N. Wilke, T. Salditt, J. Gulden, A. P. Mancuso, I. A. Vartanyants, E. Weckert, S. Schöder, M. Burghammer, and C. G. Schroer, "Hard x-ray nanobeam characterization by coherent diffraction microscopy," *Appl. Phys. Lett.* **96**(9), p. 091102, 2010.
21. C. M. Kewish, M. Guizar-Sicairos, C. Liu, J. Qian, B. Shi, C. Benson, A. M. Khounsary, J. Vila-Comamala, O. Bunk, J. R. Fienup, A. T. Macrander, and L. Assoufid, "Reconstruction of an astigmatic hard x-ray beam alignment of K-B mirrors from ptychographic coherent diffraction data," *Opt. Express* **18**(22), pp. 23420–23427, 2010.
22. C. M. Kewish, P. Thibault, M. Dierolf, O. Bunk, A. Menzel, J. Vila-Comamala, K. Jefimovs, and F. Pfeiffer, "Ptychographic characterization of the wavefield in the focus of reflective hard X-ray optics," *Ultramicroscopy* **110**(4), pp. 325–329, 2010.
23. M. Guizar-Sicairos, S. Narayanan, A. Stein, M. Metzler, A. R. Sandy, J. R. Fienup, and K. Evans-Lutterodt, "Measurment of hard x-ray lens wavefront aberrations using phase retrieval," *Appl. Phys. Lett.* **98**(11), p. 111108, 2011.
24. C. G. Schroer, P. Boye, J. M. Feldkamp, J. Patommel, D. Samberg, A. Schropp, A. Schwab, S. Stephan, G. Falkenberg, G. Wellenreuther, and N. Reimers, "Hard X-ray nanoprobe at beamline P06 at PETRA III," *Nucl. Instrum. Meth. A* **616**(2-3), pp. 93–97, 2010.
25. S. Hönig, R. Hoppe, J. Patommel, A. Schropp, S. Stephan, S. Schöder, M. Burghammer, and C. G. Schroer, "Full optical characterization of coherent x-ray nanobeams by ptychographic imaging," *Opt. Express* **19**(17), pp. 16325–16329, 2011.
26. C. G. Schroer, M. Kuhlmann, U. T. Hunger, T. F. Günzler, O. Kurapova, S. Feste, F. Frehse, B. Lengeler, M. Drakopoulos, A. Somogyi, A. S. Simionovici, A. Snigirev, I. Snigireva, C. Schug, and W. H. Schröder, "Nanofocusing parabolic refractive x-ray lenses," *Appl. Phys. Lett.* **82**(9), pp. 1485–1487, 2003.
27. A. Snigirev, V. Kohn, I. Snigireva, and B. Lengeler, "A compound refractive lens for focusing high energy x-rays," *Nature (London)* **384**, p. 49, 1996.
28. B. Lengeler, C. G. Schroer, M. Kuhlmann, B. Benner, T. F. Günzler, O. Kurapova, F. Zontone, A. Snigirev, and I. Snigireva, "Refractive x-ray lenses," *J. Phys. D: Appl. Phys.* **38**, pp. A218–A222, 2005.
29. B. Lengeler, C. Schroer, J. Tümmler, B. Benner, M. Richwin, A. Snigirev, I. Snigireva, and M. Drakopoulos, "Imaging by parabolic refractive lenses in the hard x-ray range," *J. Synchrotron Rad.* **6**, pp. 1153–1167, 1999.

Downloaded From: http://proceedings.spiedigitallibrary.org/ on 10/07/2013 Terms of Use: http://spiedl.org/terms

30. A. Schropp, R. Hoppe, J. Patommel, D. Samberg, F. Seiboth, S. Stephan, G. Wellenreuther, G. Falkenberg, and C. G. Schroer, "Hard x-ray scanning microscopy with coherent radiation: Beyond the resolution of conventional x-ray microscopes," *Appl. Phys. Lett.* **100**, p. 253112, 2012.
31. Y. Suzuki, "Resolution limit of refractive lens and Fresnel lens in x-ray region," *Japan. J. Appl. Phys.* **43**(10), pp. 7311–7314, 2004.
32. R. Hoppe, J. Reinhardt, G. Hofmann, J. Patommel, J.-D. Grunwaldt, C. D. Damsgaard, G. Wellenreuther, G. Falkenberg, and C. G. Schroer, "High-resolution chemical imaging of gold nanoparticles using hard x-ray ptychography," *Appl. Phys. Lett.* **102**(20), p. 203104, 2013.
33. A. M. Maiden and J. M. Rodenburg, "An improved ptychographical phase retrieval algorithm for diffractive imaging," *Ultramicroscopy* **109**(10), pp. 1256–1262, 2009.
34. C. G. Schroer and B. Lengeler, "Focusing hard x rays to nanometer dimensions by adiabatically focusing lenses," *Phys. Rev. Lett.* **94**, p. 054802, 2005.
35. C. G. Schroer, P. Boye, J. Feldkamp, J. Patommel, A. Schropp, A. Schwab, S. Stephan, M. Burghammer, S. Schöder, and C. Riekel, "Coherent x-ray diffraction imaging with nanofocused illumination," *Phys. Rev. Lett.* **101**(9), p. 090801, 2008.

Downloaded From: http://proceedings.spiedigitallibrary.org/ on 10/07/2013 Terms of Use: http://spiedl.org/terms